

Application of wavelet denoising to improve compression efficiency while preserving integrity of digital micrographs

T. BERNAS*†, E.K. ASEM‡, J.P. ROBINSON† & B. RAJWA†

*Department of Plant Anatomy and Cytology, Faculty of Biology and Protection of Environment, University of Silesia, Jagiellonska 28, 40-032 Katowice, Poland

†Purdue University Cytometry Laboratories, 1203 S. West State Street, West Lafayette, Indiana, U.S.A.

‡Purdue University, School of Veterinary Medicine, 625 Harrison Street, West Lafayette, Indiana, U.S.A.

Key words. Data integrity, denoising, image compression, JPEG2000, microscopy, wavelets.

Summary

Modern microscopy methods require efficient image compression techniques owing to collection of up to thousands of images per experiment. Current irreversible techniques such as JPEG and JPEG2000 are not optimized to preserve the integrity of the scientific data as required by 21 CFR part 11. Therefore, to construct an irreversible, yet integrity-preserving compression mechanism, we establish a model of noise as a function of signal in our imaging system. The noise is then removed with a wavelet shrinkage algorithm whose parameters are adapted to local image structure. We ascertain the integrity of the denoised images by measuring changes in spatial and intensity distributions of registered light in the biological images and estimating changes of the effective microscope MTF. We demonstrate that the proposed denoising procedure leads to a decrease in image file size when a reversible JPEG2000 coding is used and provides better fidelity than irreversible JPEG and JPEG2000 at the same compression ratio. We also demonstrate that denoising reduces image artefacts when used as a pre-filtering step prior to irreversible image coding.

Introduction

Digital imaging based on light microscopy has become an established technique in basic and applied biological sciences. Modern applications like high-content screening (HCS), 4D imaging, and multi-spectral imaging may involve collection of thousands of images in one experiment. Hence, such data have to be stored using efficient image-compression techniques. Several compression routines developed for digital

photography and film may be used to address this issue. Reversible compression algorithms (LZW, RLE, Huffman encoding) neither introduce distortion to images (Bernas *et al.*, 2005b) nor remove any information from images and therefore preserve the data integrity, as defined by 21 CFR part 11 (CFR, 2004). However, these reversible ('lossless') techniques can provide only a moderate compression ratio, which typically does not exceed 3:1 for biological images. More efficient compression can be obtained with irreversible ('lossy') techniques, which use fractal coding (Chen, 1998; Wohlberg & de Jager, 1999), vector quantization (Cosman *et al.*, 1994; Chen, 1998), discrete cosine transform (ISO/IEC, 1999) or wavelet transform (ISO/IEC, 2002). The last two compression schemes, described by JPEG (ISO/IEC, 1999) and JPEG2000 (ISO/IEC, 2002) standards, are the usual choice in biological microscopy owing to their widespread implementation. However, these forms of irreversible compression remove some information from images and introduce artefacts. The distortions are considered acceptable as long as the essential perceptual image quality is not decreased (Grgic *et al.*, 2003; Ebrahimi *et al.*, 2004). In other words, models of human vision are used to establish which image features are significant and consequently should be preserved (Ebrahimi *et al.*, 2004). This approach is not particularly suitable for compression of microscope images, if the data integrity is to be preserved. Therefore, to meet the requirements of 21 CFR part 11, one needs to prove that irreversible compression does not alter the outcome of analysis procedures that use images as the input data. Several validation schemes have been developed for JPEG and JPEG2000. A common approach is to establish whether the compression ratio modifies ROCs (receiver operating curves) for diagnosis based on medical images (Cosman *et al.*, 1994; Wong *et al.*, 1995; Sung *et al.*, 2002). However, the process of interpretation of the images by a clinician

Correspondence to: Tytus Bernas. Tel: +48 32 2009 484; fax: +48 32 2555 873; e-mail: tbernas@us.edu.pl.

is difficult to model and standardize (Cosman *et al.*, 1994). Therefore, this technique is expensive, time-consuming and prone to ambiguity (Cosman *et al.*, 1994; Wong *et al.*, 1995). Validation of compression algorithms is easier when automated image analysis procedures are used, owing to their reproducibility, low cost and speed. Nonetheless, the acceptable compression level is task-dependent (Wong *et al.*, 1995), regardless of whether images are analyzed by a human expert or an automated system. Furthermore, the compression level may depend on image quality (Sung *et al.*, 2002). This parameter, in turn, depends on the image-registration system and the properties of the imaged specimen. Consequently, it may be necessary to re-validate an irreversible compression scheme if any of the three components (imaging system, interpretation/analysis procedure or task) is changed. These problems may be obviated if an algorithm for compression of microscope images is constructed without reference to human vision models and validated in a way that is independent of the image-analysis task.

Instead of studying the result of interpretation/analysis of compressed images, one may focus on the information content of the input data. The information content of a micrograph is limited by the presence of instrumental noise, which constitutes part of image data. Removal of this redundant noise component is an obvious method to decrease size of image data (perform image compression). Numerous and efficient schemes of removal signal-independent (Gaussian) noise with wavelet shrinkage (thresholding) have been developed and tested using several types of images (Donoho & Johnstone, 1994; Donoho, 1995; Simoncelli, 1999; Chang *et al.*, 2000). These have been also used to remove signal-independent (Poisson) noise from images subjected to variance-stabilizing transformation with a normal approximation (Donoho, 1993; Fryzlewicz & Nason, 2001). Alternatively, one may adapt wavelet shrinkage with original Poisson counts (Kolaczyk, 1997; Kolaczyk, 1999b; Nowak & Baraniuk, 1999) or use Bayesian inference (Kolaczyk, 1999a; Timmermann & Nowak, 1999) to remove this type of signal-independent noise. Nonetheless, application of denoising for compression of biological light micrographs has not been extensively evaluated up to the author's knowledge. One may note that, in contrast to natural scene images, there are no established universal measures of image quality.

Therefore, to establish an irreversible, yet data-preserving compression mechanism, we use previously developed model of noise, which is a function of signal in our imaging system (Bernas *et al.*, 2005a). Then, we implement an unbiased Poisson noise estimator in wavelet domain (Nowak & Baraniuk, 1999) and combine it with an adaptive wavelet shrinkage scheme (Sendur & Selesnick, 2002). We demonstrated previously that proposed denoising procedure combined with reversible JPEG2000 coding results in a decrease of microscope image (Bernas *et al.*, 2006). In this paper, we evaluate the effects of application of this

compression method on possible distortion of microscope modulation transfer function (MTF) and actual biological fluorescence micrographs. We compare fidelity of proposed denoising/coding scheme to fidelity provided by irreversible JPEG2000 and JPEG in the same conditions. We also study fidelity of proposed denoising combined irreversible JPEG2000 coding.

Materials and methods

Computer software and hardware

Image processing and analysis procedures were executed using an AMD Athlon XP 2800+ (1950 MHz) machine equipped with 1 GB DDR RAM (333 MHz) and a RAID 0 matrix comprising two ATA 133 hard drives. The calculations were performed with Matlab R13 (MathWorks) running under MS Windows 2000 (SP4).

Registration of microscope images and construction of model images

Cell culture and confocal microscopy. Transformed human fibroblasts MSU 1.1 were cultured, stained with propidium iodide (PI) and imaged using a Bio-Rad MRC 1024 confocal microscope as described previously (Bernas *et al.*, 2004). PI fluorescence was detected using photomultipliers in photon-counting mode. The array test pattern on a microscope test slide (Richardson Technologies Inc., Bolton, Canada) was imaged using the same confocal system. The images were registered at the focal plane of maximum intensity using reflected light (488 nm) as described in Bernas *et al.* (2006). Light intensity was registered with 8-bit precision. The images were sampled close to Nyquist spatial frequency (approximately seven image pixels corresponded to one Airy disc diameter). Hence, according to Rayleigh criterion, one could resolve two point objects if they were at least 3.5 pixels apart.

Generation of model images of sinusoidal test patterns. To test the influence of irreversible compression schemes on the effective modulation transfer of an optical microscope, sequences of synthetic images (512×512 pixels, 8 bit) containing vertical sinusoidal test patterns were generated (Fig. 1). A sequence comprised the patterns characterized by the period from 2 (T_{\min}) to 128 (T_{\max}) pixels. The minimum intensity (amplitude) was set to 0, whereas the maximum intensity was calculated for each pattern using the approximate formula for microscope MTF (Stokseth, 1969):

$$I_{\max} = N_{\max} \times (1 - 0.69f + 0.0076f^2 + 0.04f^3)^2,$$

where

$$f = 2 * \left(\frac{1}{T} - \frac{1}{T_{\max}} \right) \left(\frac{1}{T_{\min}} - \frac{1}{T_{\max}} \right)^{-1}, \quad (1)$$

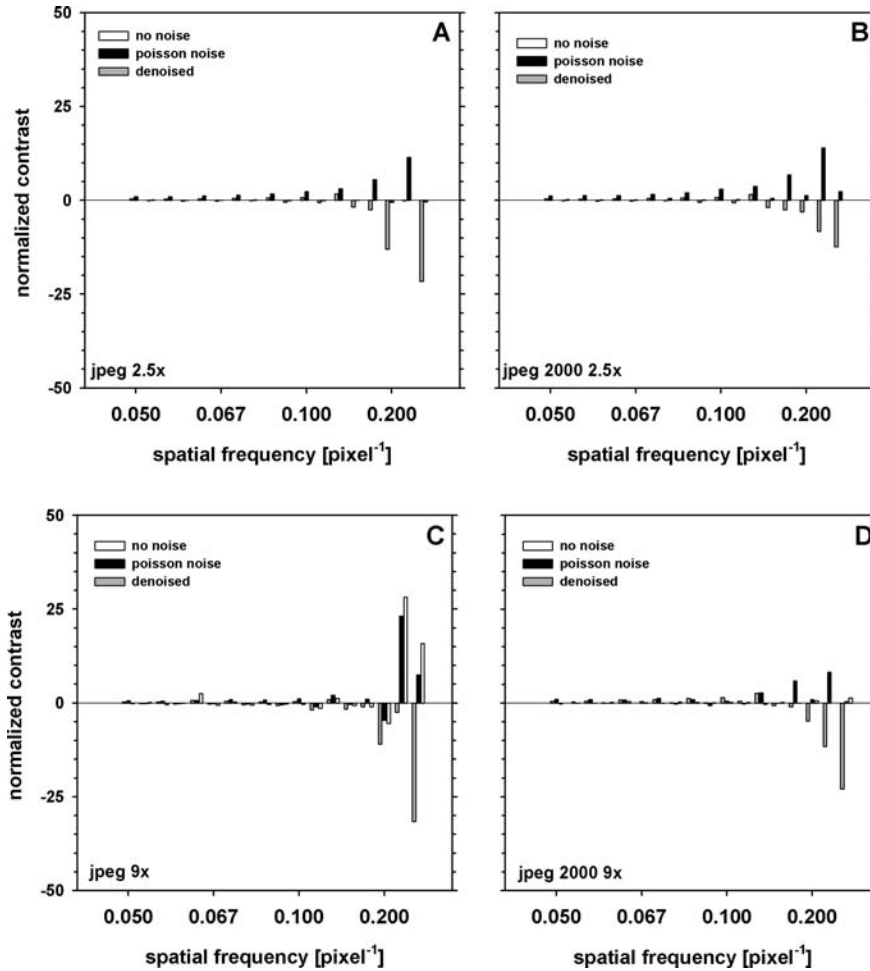


Fig. 1. Influence of compression on the effective MTF in an imaging system where a high maximal number of photons (200) was registered. The MTF was represented by a series of images of sinusoidal test patterns without noise (white bars), with Poisson noise (grey bars) or with Gaussian noise (black bars). A negative contrast value indicates a decrease in the energy of a spatial frequency, whereas a positive contrast value indicates an increase of the energy. The images were compressed using irreversible JPEG2000 (A and C) and JPEG (B and D), with a compression ratio of $6\times$ (A and B) or $18\times$ (C and D).

where f is the normalized spatial frequency, T the spatial period of the sinusoidal pattern, T_{\min} , T_{\max} the minimum (2) and maximum (128) values of T , N_{\max} the maximum photon number (50 or 200) and I_{\max} the maximum intensity.

The calculations were performed using 64-bit numbers (IEEE floating point), and the results (I_{\max}) were rounded to 8-bit integers. The maximum intensity (I_{\max}) decreases with increasing spatial frequency (decreasing spatial period). Therefore, the image sequence represents the MTF of a confocal microscope. Two such sequences were generated with N_{\max} set to 50 or 200 to simulate images registered with low and high photon numbers, respectively.

SNR estimation and image compression in wavelet domain

It has been demonstrated that the image-compression ratio can be improved through a suitable denoising procedure (Chang *et al.*, 2000). The greatest part of the noise present

in microscope images is caused by inherent variation in the arrival rate of photons owing to the quantum nature of light. We demonstrated previously that the noise present in the biological micrographs registered with our imaging system is signal-dependent and may be adequately described using Poisson model (Amer *et al.*, 2002; Bernas *et al.*, 2005a). Thus, an unbiased Poisson noise estimator [described in Nowak & Baraniuk (1999)] is combined with the bivariate wavelet-shrinkage algorithm (Sendur & Selesnick, 2002) to perform image denoising. Briefly, two forward wavelet transforms (three decomposition levels) of images are calculated using a bi-orthogonal 3.3 wavelet:

$$S_I = \sum_{k,l} w_I(k,l)\lambda(k,l), \quad (2)$$

where S_I is the i th wavelet coefficient (signal), $w_I(k,l)$ bi-orthogonal wavelet, $\lambda(k,l)$ the image intensity, l and k the image spatial coordinates and squared bi-orthogonal 3.3

wavelet:

$$\sigma_I^2 = \sum_{k,l} w_I^2(k,l)\lambda(k,l), \quad (3)$$

where σ_I^2 is the noise variance associated with the i th wavelet coefficient, $w_I^2(l,k)$ is the squared bi-orthogonal wavelet as described in Nowak & Baraniuk (1999). This procedure provides an unbiased estimate of noise calculated separately for each wavelet coefficient. The original wavelet shrinkage scheme described in Nowak & Baraniuk (1999) did not take advantage of the fact that wavelet coefficients at different resolution scales (but corresponding to the same image region) are correlated. Hence, to exploit correlation between respective detail coefficients at finer (child) and coarser (parent) scales, wavelet shrinkage algorithm described in Sendur & Selesnick (2002) was applied instead. Briefly, large child coefficients, which do not correspond to large parent coefficients, are likely to represent only noise and therefore are decreased. The shrinkage procedure is constructed using the following set of equations:

$$S_{Ic} = R_{Ic} \left(1 + \frac{\sqrt{3}\sigma_{Ic}^2}{\delta_c^2 r} \right) = R_{Ic} F_c$$

$$S_{Ip} = R_{Ip} \left(1 + \frac{\sqrt{3}\sigma_{Ip}^2}{\delta_p^2 r} \right) = R_{Ip} F_p,$$

where

$$r = \sqrt{\left(\frac{R_{Ic}}{\delta_c}\right)^2 + \left(\frac{R_{Ip}}{\delta_p}\right)^2} \quad (4)$$

and

$$\delta_c^2 = \frac{1}{N_c^2} \sum_{n \in C} S_{In}^2$$

$$\delta_p^2 = \frac{1}{N_p^2} \sum_{n \in P} S_{In}^2,$$

where S_{Ic} and S_{Ip} are the initial child and parent wavelet coefficients, R_{Ic} and R_{Ip} , the resulting (shrunk) child and parent wavelet coefficients, σ_{Ic}^2 and σ_{Ip}^2 , the child and parent noise variances, δ_c^2 and δ_p^2 , the variances of distributions of wavelet coefficients belonging to child (c) and parent (p) sub-bands and N_p and N_c the number of child and parent coefficients.

These equations cannot be solved in an analytical way to give the wavelet shrinkage functions. Thus, the shrinkage is executed in an iterative manner using an algorithm based on (Sendur & Selesnick, 2002):

1. Initialize parameters: $k = 1$, $R_{Ic}^k = S_{Ic}$, $R_{Ip}^k = S_{Ip}$
2. Calculate r , F_p and F_c using R_{Ic}^k , R_{Ip}^k
3. Find R_{Ic}^{k+1} , R_{Ip}^{k+1} using $R_{Ic}^{k+1} = R_{Ic}^k / F_c$ and $R_{Ip}^{k+1} = R_{Ip}^k / F_p$
4. Calculate the absolute differences; $\varepsilon_c = |R_{Ic}^{k+1} - R_{Ic}^k|$, $\varepsilon_p = |R_{Ip}^{k+1} - R_{Ip}^k|$

5. If $\varepsilon_c < 1$ and $\varepsilon_p < 1$, then set $R_{Ic} = R_{Ic}^k$ and terminate; otherwise set $k = k+1$, $R_{Ic}^k = R_{Ic}^{k-1}$, $R_{Ip}^k = R_{Ip}^{k-1}$ and go to step 2

This procedure is executed with the wavelet coefficients at first and second decomposition levels constituting the parent and the child sub-bands, respectively. Following shrinkage, a reverse wavelet transform is executed on S_I :

$$\lambda^d = w^{-1} S^d \quad (5)$$

where S^d is the denoised wavelet image representation, w^{-1} the inverse wavelet transform and λ^d the denoised image.

One should note that in original wavelet shrinkage procedure described in Sendur & Selesnick (2002) was constructed to remove only signal-independent (Gaussian) noise. Therefore, to validate the proposed method, the signal intensity was calculated as an average from the resulting (denoised) images over the regions where the pixel value was greater than 30. The absolute difference between the denoised and initial images in these regions was used as an estimate of the noise level and compared to a noise estimate obtained with independent technique, as described in our earlier papers (Bernas *et al.*, 2005a; Bernas *et al.*, 2006). We demonstrated that change of pixel intensity introduced by the proposed algorithm follows expected Poisson characteristics with respect to dependence on remaining signal and the noise magnitude (Bernas *et al.*, 2005a; Bernas *et al.*, 2006).

Wavelet compression and coding. Execution of the wavelet-shrinkage algorithm results in zeroing of some wavelet coefficients in the denoised image, as described earlier. The zeroed coefficients represented noise modelled by Poisson distribution. This information-preserving noise removal constitutes the irreversible ('lossy') step of the compression algorithm. This procedure is followed by reversible ('lossless') image coding using a wavelet representation (format), which is part of the JPEG2000 specification (ISO/IEC, 2002). Where indicated, irreversible JPEG2000 compression was used. Both procedures were executed using JasPer (<http://www.ece.uvic.ca/~mdadams/jasper/>).

Estimation of image distortion in compression

Alteration of effective microscope MTF. The sequences of the pattern images were compressed using JPEG or coded with reversible or irreversible JPEG2000. The contrast between the minima and maxima of these test patterns was calculated as total difference between the image and its copy shifted horizontally by the distance equal to the pattern period. The contrast was then normalized to the value obtained for the non-compressed counterparts of these pattern images using the formula:

$$C_n = \frac{\sum_{i,j} |I_{cm}(i,j) - I_{cm}(i+s,j)|}{\sum_{i,j} |I_{noc}(i,j) - I_{noc}(i+s,j)|} - 1 \quad (6)$$

where C_n is the relative contrast, i and j are horizontal and vertical pixel coordinates, s is the profile shift (equal to the half of the spatial period) and I is the pixel intensity in compressed (cm) and non-compressed (noc) images.

Similar calculations were performed on the sequences of pattern images to which Poisson was added and on their denoised counterparts. The normalized contrast was plotted against the spatial frequency (inverse of the spatial period, T). Note that the relative contrast was equal to zero if no artefacts were introduced by a compression algorithm, negative when a spatial frequency was attenuated and positive when the frequency was enhanced.

Artefacts in microscope images of test specimens. Artefacts introduced by image compression were estimated using a test slide (Richardson Technologies) containing horizontal array patterns, composed of bars 0.250 μm , 0.125 μm or 0.100 μm wide. Intensity profiles (3-pixel width) were measured from images of the patterns registered with either a large or a small number of photons. The normalized contrast between the profile minima and maxima was calculated using Eq. 6 (with $j_c - 1 < j <= j_c + 1$, where j_c is the vertical coordinate of the centre of the intensity profile).

Changes in fluorescence intensity distributions in biological images. To establish whether compression introduced changes in the total fluorescence intensity distributions, the 'earth mover's' distance (EMD) algorithm (Rumner *et al.*, 2000) was used to compare image histograms between reference and compressed images. Briefly, the minimal average (per pixel) intensity change needed to transform histograms of a compressed image into the respective histogram of an uncompressed (reference) image was computed for every such image pair.

Alterations of spatial fluorescence distribution in biological images. To verify whether compression produced local intensity changes in spatial fluorescence distributions of the nuclei in uncompressed and compressed images were studied. The spatial distributions were compared using texture parameters (features): grey-level co-occurrence matrix (Haralick), gradient-based features, run-length matrix parameters and wavelet energy. These parameters were calculated using MaZda 3.2 (Materka & Strzelecki, 1998) and are described in detail in Materka & Strzelecki (1998) and Tuceryan *et al.* (1998). The grey-level co-occurrence parameters were calculated at 1, 2, 3, 4 and 5-pixel distance. The gradient-based features and run-length matrix parameters were calculated at 45, 90 (vertical), 135 and 180 (horizontal) degrees. The wavelet energy was calculated at first, second and third decomposition levels. Calculations were performed in the areas where the fluorescence intensity was higher than 30 (background) using 8 bits of dynamic range. The texture parameters of images compressed using JPEG and JPEG2000 (with and without denoising) were divided by the respective values for their non-compressed counterparts. Two

sets of images (raw vs. denoised and coded with reversible JPEG2000), each characterized with 275 normalized texture parameters were subjected to step-wise discriminant analysis. Wilk's lambda was used to establish the parameters with the highest discriminant power. The parameters were added to and removed from the analysis set using probability of F (0.05 for entry and 0.10 for removal).

Results

Influence of irreversible compression schemes on the effective MTF

Effects of irreversible compression with JPEG and JPEG2000 were analyzed using sequences of model images containing sinusoidal patterns representing several spatial frequencies. As expected, no distortions were generated when noiseless (pattern) images were coded ($2.5\times$ compression ratio) with reversible JPEG2000 (Figs 1(B) & 2(B)). Only minor distortions were generated by irreversible JPEG at the same compression ratio (Figs 1(A) & 2(A)). However, enhancement of high spatial frequencies was observed when images contaminated by Poisson noise were compressed with JPEG or JPEG2000 (Figs 1(AB) & 2(AB)). One should note that irreversible variant of the latter algorithm was used to obtain the same compression ratio ($2.5\times$). Removal of the Poisson noise with the proposed denoising procedure resulted in attenuation of the highest spatial frequencies (Figs 1(AB) & 2(AB)). It should be noted that MTF distortion was smaller when denoising was combined with reversible JPEG2000 than when irreversible JPEG was used (compare panels A and B in Figs 1 & 2). Moreover, both attenuation and enhancement were less manifested in bright images (higher number of photons and SNR) than in dark images (lower number of photons and SNR, compare Figs 1 & 2, panels AB).

High compression ratios ($9\times$) resulted in a marked increase of distortions (Figs 1(CD) & 2(CD)). Small enhancement of certain spatial frequencies was observed in noiseless images (one should note that only irreversible coding was used at this stage). Compression of images containing Poisson noise resulted in attenuation of some spatial frequencies, whereas some were enhanced (Figs 1(CD) & 2(CD)). This effect was more pronounced at high than at low frequencies. By contrast, no enhancement but only attenuation of high spatial frequencies was observed when noise was removed prior to coding with irreversible JPEG2000 (Figs 1(CD) & 2(CD)). Similarly to low compression ratio ($2.5\times$) MTF distortions in highly compressed ($9\times$) images were more manifested at low number of photons (low SNR) than at high number of photons (high SNR). Furthermore, reversible JPEG2000 offered better fidelity (lesser MTF distortion) than irreversible JPEG2000 (at the same compression ratio).

In general, it may be concluded that irreversible image compression produces alterations of effective microscope MTF. The magnitude of distortions increases with spatial

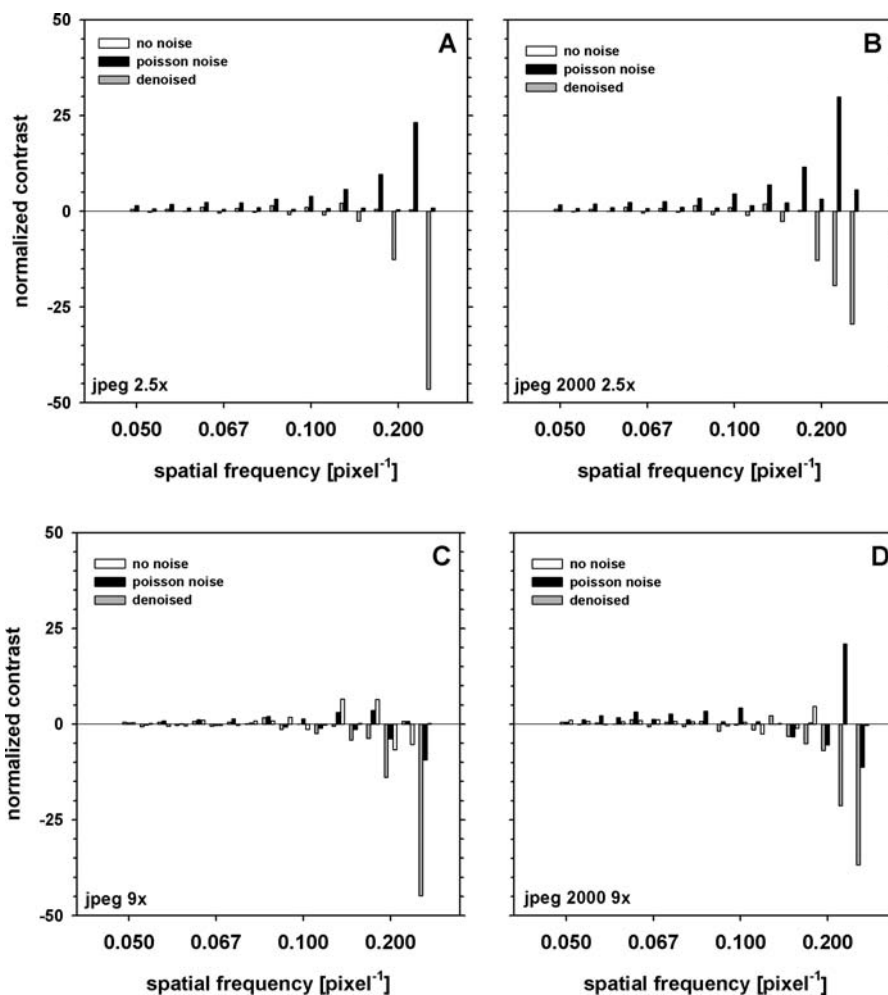


Fig. 2. Influence of compression on the effective MTF in an imaging system where a low maximal number of photons (50) was registered. The MTF was represented by a series of images of sinusoidal test patterns without noise (white bars), with Poisson noise (grey bars) or with Gaussian noise (black bars). A negative contrast value indicates a decrease in the energy of a spatial frequency, whereas a positive contrast value indicates an increase of the energy. The images were compressed using irreversible JPEG2000 (A and C) and JPEG (B and D), with a compression ratio of $6\times$ (A and B) or $18\times$ (C and D).

frequency. The presence of Poisson noise aggravates the problem, which becomes more severe as SNR decreases. Removal of the noise with the proposed algorithm resulted in a decrease in magnitude of distortions at the expense of attenuation of the highest spatial frequencies. However, no enhancement of spatial frequencies was observed in denoised images. This notion suggests that the application denoising results in removal of small image details (corresponding to frequencies close to MTF cut-off) and prevents introduction of image artefacts of similar size. Furthermore, one may expect application of denoising would produce a decrease in image file size. Therefore, denoising followed by JPEG2000 coding (either reversible or irreversible) seems optimal strategy for compression of light micrographs. This strategy was implemented and tested in practice of biological fluorescence microscopy, as described in the next paragraphs.

Performance of wavelet-shrinkage followed by reversible (lossless) JPEG2000 coding

Biological images. A set of fluorescence images of PI-stained nuclei was denoised using the proposed algorithm (see Materials and Methods) and compressed using the reversible JPEG2000 encoding, as illustrated in an example in Fig. 3. No gross artefacts were generated and efficient compression was achieved. Presence of artefacts at compression ratios were studied in detail using a set of 470 images containing varying numbers of nuclei and characterized by different intensity levels.

The compression ratios increased with decreasing fluorescence intensity (data not shown). As expected, the reversible JPEG2000 coding preceded by denoising exhibited higher compression efficiency than the reversible JPEG2000 coding (the most efficient lossless compression method) alone

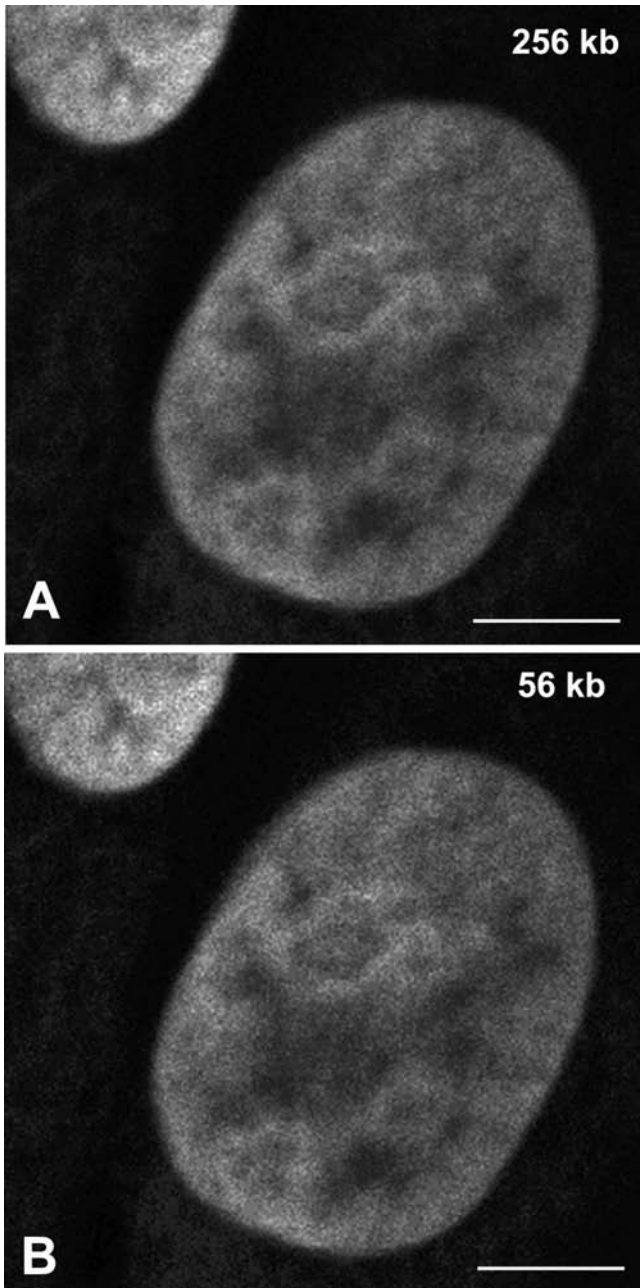


Fig. 3. Effects of wavelet-based denoising (shrinkage) on a representative image of a cell nucleus stained using propidium iodide (PI). File sizes of the raw (A, saved as TIFF) and denoised (B, encoded using the reversible JPEG200) images are shown in kilobytes (kb). Bar – 5 μm . The image is reproduced from the Figure 4 presented in Bernas *et al.* (2006).

(Fig. 4). Detailed information on application this and similar techniques for compression of biological micrographs were published in previous papers (Bernas *et al.*, 2005a; Bernas *et al.*, 2006).

The compressed images were compared quantitatively to their uncompressed counterparts with respect to the intensity

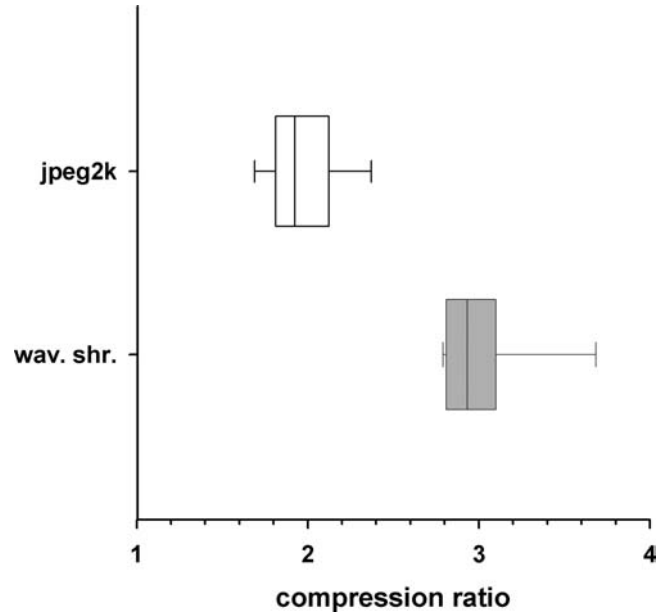


Fig. 4. Overall compression efficiency of the reversible JPEG2000 with (grey) and without (white) wavelet shrinkage. Data range indicated with bars, 10th and 90th percentiles with boxes and median compression ratios with vertical lines. The data are extracted from Figure 6 in Bernas *et al.* (2006).

distribution (histogram). Average EMD (see Materials and Methods) was equal to 1.18 ± 0.14 (see also Table 1), which indicated that the denoising did not introduce gross changes to histograms.

Possible changes in spatial fluorescence distribution within cell nuclei were analyzed using the Haralick texture parameters (entropy, sum of squares and difference variance) and wavelet energy (first and second decomposition levels). These features were chosen so as to provide the highest discriminative power between sets of image compressed using different algorithms (as discussed further, see also Materials and Methods). The wavelet denoising resulted in only a slight decrease of entropy (a measure of information, Fig. 5(A)). The decrease was more pronounced at a 2- than at a 5-pixel distance, which indicates that the finer (smaller than Rayleigh resolution distance, see Materials and Methods) details were affected more than the coarser (larger but close to Rayleigh resolution distance) details. The sum of squares (a measure of intensity distribution width) was slightly decreased by the denoising at both distances (Fig. 5(B)). A larger decrease was observed in the case of the difference variance (a measure of contrast, Fig. 5(C)). One should note that the finer (2-pixel distance) details were more affected than the coarser (5-pixel distance). Effects of the denoising on the texture of cell nuclei were studied using the wavelet energy coefficients at the first (Fig. 6(A)) and second (Fig. 8(B)) decomposition levels. A slight decrease in energy vertical (HL) and horizontal (LH) spatial frequencies was observed at the second decomposition

Table 1. Alterations of fluorescence intensity distributions (histograms) in irreversible compression, as measured using EMD. Data are expressed as the average \pm standard deviation.

Compression method	Compression ratio: relative to reversible JPEG2000 with denoising and absolute median (in parentheses)		
	1 (2.5 \times)	3 (7.5 \times)	9 (22.5 \times)
JPEG2000 with denoising	1.18 \pm 0.14	1.17 \pm 0.16	1.19 \pm 0.17
JPEG2000 without denoising	0.09 \pm 0.02	0.15 \pm 0.04	0.20 \pm 0.10
JPEG	0.04 \pm 0.01	0.17 \pm 0.04	0.78 \pm 0.13

level (Fig. 6(B)). This fact indicates that the 4-pixel details were not affected in any significant degree. Greater decrease was noted in the case of spatial frequencies between 2 and 4 pixels (Fig. 6(B), HH), at 2 pixels (Figs 6(A), HL and LH) and higher (Figs 6(A), HH)). This notion indicates that details smaller than Rayleigh resolution distance were removed by the wavelet denoising procedure. The opposite effect occurred when irreversible algorithms (JPEG2000 and JPEG) were used (as discussed in the next section). One may conclude that the wavelet shrinkage resulted in removal of noise, but did not significantly affect the details of objects that could be resolved using our imaging system. To validate this notion, we used a microscope test slide containing an array pattern.

Microscope test patterns. Denoised images of an array grid pattern were compared with their raw counterparts to estimate the influence of wavelet shrinkage (wavelet-based denoising) followed by reversible JPEG2000 encoding on the reproduction fidelity of details of known size. The result was quantified on the basis of contrast between the reflective and transparent regions of the microscope test patterns (see Materials and Methods), as shown in Fig. 7. Wavelet shrinkage introduced a slight decrease of the contrast in the images of the finest (0.100 μm , Fig. 7(A)) and a coarser (0.125 μm , Fig. 7(B)) array grating. Compression with JPEG and irreversible JPEG2000 (without denoising) resulted in an increase of the contrast of the finest and coarser patterns. The increase was prominent when images were registered using a small number of photons (Fig. 7, grey bars) and compressed using JPEG2000. Similar changes in contrast were manifested at both short (one-bar length) and long pattern shift (three-bar lengths, data not shown). The increase in contrast indicates that the artefacts were introduced into the whole pattern at regular intervals (i.e. they were periodic). Both JPEG2000 variants (reversible and irreversible) exhibited better reproduction fidelity of the coarser (0.125 μm) array than of the finest (0.100 μm) grating. As expected, the best fidelity for the two test patterns was achieved when wavelet shrinkage was followed by JPEG2000. The coarsest pattern (0.250 μm) was reproduced accurately by all the algorithms (Fig. 7(C)), regardless of whether denoising was applied or not. Similar data regarding application of this and other algorithms

for compression of test pattern images were also presented in Bernas *et al.* (2006).

Performance of wavelet-shrinkage followed by irreversible (lossy) JPEG2000 coding

The results presented in the previous section led us to hypothesize that the wavelet denoising, implemented as a pre-filtering step, may reduce artefacts generated by irreversible compression schemes like JPEG2000. Hence, in order to verify this notion, the set of fluorescence images of PI-stained nuclei was denoised and subsequently encoded using the irreversible JPEG2000. The effects of this procedure were compared with compression using JPEG and JPEG2000 alone.

Biological images. Small values of the average EMD (Table 1, see Materials and Methods) indicate that irreversible compression with the ratios used did not introduce major alterations in the image histograms. Interestingly, the largest nominal changes were observed when wavelet denoising was used. However, the average EMD was not affected by the final compression ratio if the denoising step was implemented. Hence, one may conclude that changes in the histogram resulted from the noise removal, not the subsequent irreversible coding. By contrast, average EMD increased steadily with compression ratio when JPEG or irreversible JPEG2000 was used without denoising (the increase is higher for JPEG than JPEG2000). These facts indicate that in the presence of noise, histogram distortions are introduced by irreversible compression, and the magnitude of the distortions depends on the compression ratio.

Changes in spatial fluorescence distribution in cell nuclei were analyzed using the Haralick texture parameters, as before. At the lowest (2.5 \times) compression level, wavelet denoising resulted in a decrease in average relative values of the sum of squares (Fig. 8(A), a measure of intensity distribution width), the entropy (Fig. 8(D), a measure of information) and the difference variance (Fig. 8(G), a measure of contrast). The change of entropy was the smallest, whereas that of sum of squares the largest of the three. One should note that the decrease in the sum of squares and difference variance was more pronounced at a 2-pixel distance than at a 5-pixel

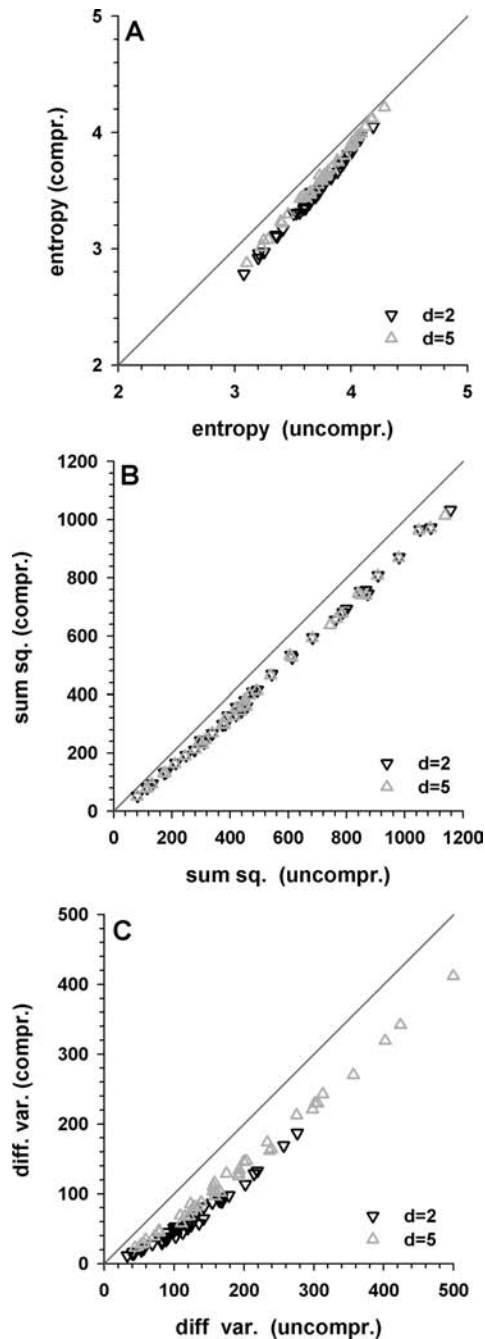


Fig. 5. Influence of wavelet denoising on textures in the images of PI-stained nuclei, determined using Haralick parameters: entropy (A), sum of squares (B) and difference variance (C). The parameters were calculated at distances of 2 (black triangles) and 5 (grey triangles) pixels. For clarity, only 10% of points (randomly chosen) are shown. The diagonals (indicating unchanged parameters) are depicted with dark grey lines.

distance. Application of irreversible compression schemes (JPEG and JPEG2000) without wavelet denoising resulted in a small increase of the three texture parameters. This effect was most pronounced for the difference variance (Fig.

8(G)). Furthermore, the increase of the difference variance was greater at a 2-pixel distance than at a 5-pixel distance. This observation indicates that small details (below the resolution limit of the imaging system) may be enhanced in the images compressed with JPEG and irreversible JPEG2000. At the medium ($7.5\times$) compression level, a greater increase in the values of the texture parameters occurred when JPEG2000 without denoising was used (Fig. 8(BEH)). By contrast, when JPEG was used, a decrease was observed. The highest ($22.5\times$) compression resulted in a marked decrease in the sum of squares, the entropy and the difference variance regardless of the algorithm used (Fig. 8(CFI)). One should note that when wavelet denoising was used, the compression level did not affect the magnitude of the decrease. By contrast, when JPEG and irreversible JPEG2000 (without denoising) were used, transitions from positive to negative values of the texture parameters were observed. A similar pattern was revealed when wavelet energy was used to analyze texture of the nuclei. At the low compression level, the standard methods (without denoising) caused a slight increase in the wavelet energy corresponding to small (not resolvable) details (Fig. 9(AB)). Greater enhancement was observed at medium compression (Fig. 9(CD)). This effect was most prominent for spatial frequencies between 2 and 4 pixels (Fig. 9(D), HH), 2 pixels (Fig. 9(C), HL & LH) and higher than 2 pixels (Fig. 9(C), HH). Use of the irreversible algorithms with the highest compression ratios resulted in a decrease in wavelet energy of all but the lowest spatial frequencies (Fig. 9(F), HL & LH bands). One should note that in the denoised images, the textures of the nuclei were, in general, not influenced by the compression level (Compare Fig. 9(AB)–(EF)). A change could be detected only in the highest spatial frequencies in the images compressed with the highest ratios (Fig. 9(E)). Thus, one may conclude that JPEG and irreversible JPEG2000 compression schemes introduced artefacts into images containing Poisson noise. Furthermore, irreversible compression not preceded by denoising might remove some image content, which is not identified as noise. The resultant image distortion is a net product of these two effects as illustrated in the Figs 10(C) and (D). The obtained results strongly suggest that the proposed method of wavelet-based denoising helps preserve data integrity in microscope images that are subsequently compressed with irreversible JPEG2000. To validate this notion, we again used the microscope test slide with an array grid pattern.

Images of microscope test patterns compressed with irreversible JPEG2000 coding. The procedure described for reversible JPEG2000 coding (Fig. 7) was repeated using irreversible JPEG2000 (with or without denoising) and JPEG. Compressed images were compared with their raw counterparts to estimate the fidelity of reproduction of details of known sizes. The fidelity of reconstruction was quantified on the basis of the contrast between reflective and transparent regions of

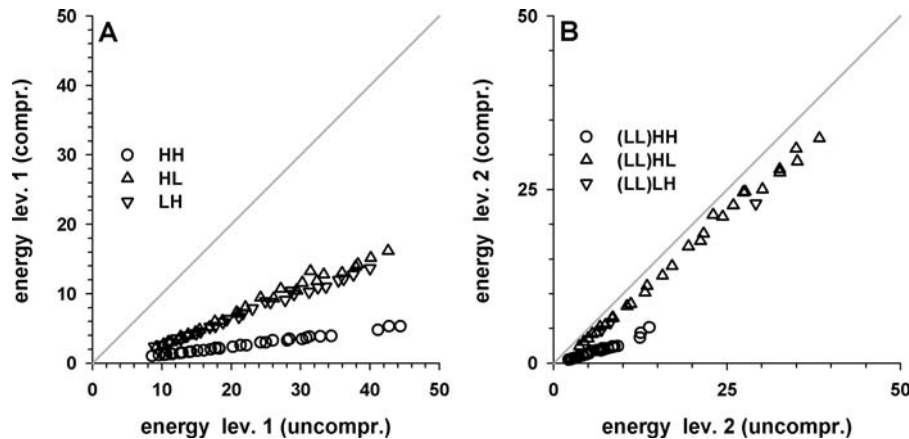


Fig. 6. Influence of wavelet denoising on textures in the images of PI-stained nuclei, determined using wavelet (Haar) decomposition. The relative wavelet energy was measured at first (A) and second (B) decomposition levels, following application of high-pass (H) and low-pass (L) filters in sequence.

the patterns (see Materials and Methods). Only slight changes in the relative contrast of the finest (0.100 μm , Fig. 11(A)) pattern were observed at moderate compression ratio (7.5 \times). However, an increase in the contrast of the coarser (0.125 μm , Fig. 11(C)) pattern was observed in the images compressed with JPEG2000 without denoising. JPEG2000 used with a high compression ratio (approximately 22.5 \times) resulted in a marked decrease in contrast of the fine and coarser patterns registered with a small number of photons (Figs 11(B) and (D), respectively). However, an increase in the contrast was observed when JPEG was used. It was also observed that high spatial frequencies (represented by the fine and the coarser patterns) were significantly attenuated at the highest compression level of JPEG (Figs 11(B) and (D), respectively). This effect was emphasized when the number of photons was low. Comparing results of compression at low (Fig. 7), moderate (Fig. 11(ACE)) and high (Fig. 11(BDF)) ratios, it was observed that if JPEG or JPEG2000 is used (both without the denoising step), high spatial frequencies that were initially enhanced became attenuated as the ratio increased. This observation indicates that periodic artefacts were introduced at low compression levels. By contrast, if wavelet denoising was applied before JPEG2000 encoding, only continuous attenuation or no change was detected. As expected, the distortions introduced by the irreversible encoding were smaller in the case of denoised images than in the case of original images.

Discussion

Current irreversible ('lossy') compression schemes are optimized to preserve perceptual image quality. Consequently an 'information-preserving' algorithm, as understood by ACR/NEMA standard (National Electrical Manufacturers, 2004), retains all the significant information when it is 'visually lossless'. Efforts to meet this requirement resulted in development of JPEG2000 to supersede the

older JPEG. Nonetheless, the latter is still the accepted industry standard for irreversible compression of images registered with light microscopy owing to its implementation in numerous microscopy-related packages used by cell biologists, pathologists, and microbiologists. Even though perceptual image quality is not decreased (Grgic *et al.*, 2003; Ebrahimi *et al.*, 2004), application of both JPEG and irreversible JPEG2000 may cause detectable alterations in image characteristics. We used synthetic images and a microscope specimen comprising a periodic test pattern to demonstrate that such distortions are reflected in the effective MTF. Therefore, use of irreversible compression will affect every kind of image data generated by biological microscopy. The magnitude and type distortions were dependent on compression ratio, spatial frequency and SNR. Although at a low compression ratio, enhancement of the highest spatial frequencies (transferred by a microscope) was observed, both attenuation and enhancement of the frequencies in this range were detectable when the ratio was high. Closer examination of real microscope data revealed that in some image regions, small image details were introduced, whereas in others details of the same scale were removed. One may note that the former effect corresponded to enhancement of high spatial frequencies (high-pass filtering), whereas the latter to their attenuation (low-pass filtering). It is not surprising that the distortions were most pronounced when the number of registered photons (and SNR) was low.

We demonstrated that the MTF distortions could be mitigated if the noise was removed. Moreover, denoising reduces the amount of memory required to encode an image by discarding a part which can be proved not to carry information on the imaged object. Therefore, this procedure may assist the operation of standard compression algorithms while preserving integrity of image data. We ascertained that the proposed denoising method did not introduce any artefacts to the images of periodic grating arrays. The response of an imaging system to such patterns is an

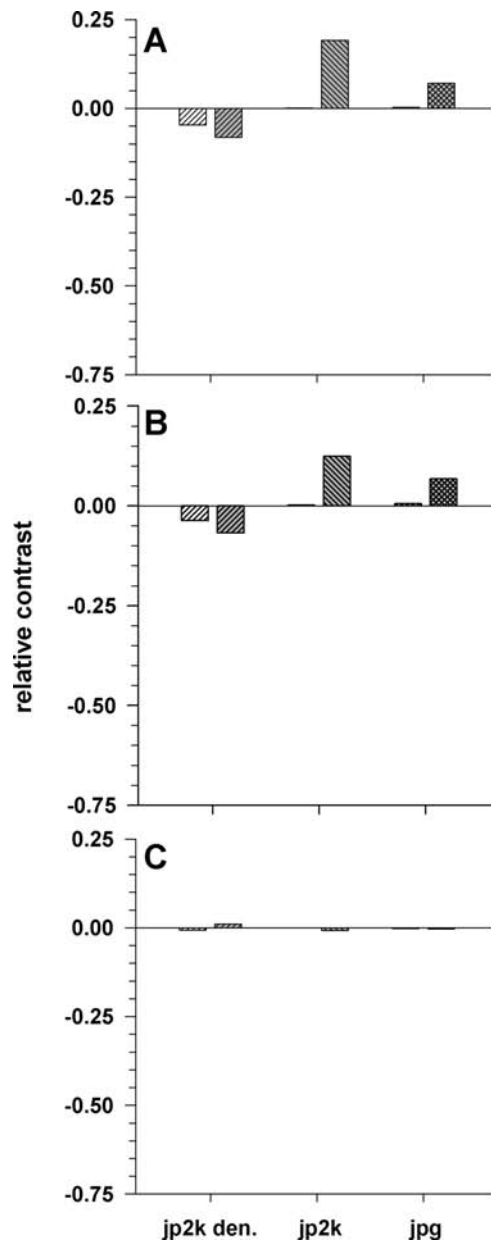


Fig. 7. Influence of irreversible compression on images of the array test pattern registered with large (average of 72.8 per pixel, white bars) and small (an average of 4.1 per pixel, dark bars) number of photons. The fidelity of reproduction of the test pattern was estimated using relative contrast between the bright and dark bars (see Materials and Methods). The contrast was calculated shifting the pattern with respect to itself by one bar width. The respective widths were 0.100 μm (A), 0.125 μm (B) and 0.250 μm (C). The wavelet denoising followed by the reversible JPEG2000 is shown with a slash pattern. Effects of compression (with the same ratio as obtained using the denoising) using JPEG (backslash pattern) and JPEG2000 (grid pattern) are shown for comparison. These data were also presented in (Bernas *et al.*, 2006) in Figs 8 and 9 (one should note that data in this work are shown with offset of -1).

estimate of the MTF. The finest of the patterns (bar thickness 0.100 μm) was characterized by a spatial frequency of 5.0 μm^{-1} , which was close to the microscope cut-off frequency (5.7 μm^{-1}). Therefore, it was concluded that wavelet denoising does not impair the resolution of microscope imaging. We validated this approach for biological images using objective and human-independent measures of fidelity. We demonstrated that wavelet shrinkage followed by lossless JPEG2000 coding did not introduce significant changes to the intensity distributions, as indicated by a small EMD (comparable with the intensity resolution). Furthermore, changes in texture of cell nuclei were consistent with removal of sub-resolution details (which, by definition, represented only noise).

Increase of compression ratio could be achieved by using the wavelet denoising with irreversible JPEG2000. Such a procedure did not prevent removal of fine details (represented by high spatial frequencies). Nonetheless, when JPEG and irreversible JPEG2000 (without denoising) were used to obtain a similar compression ratio, both removal of image details and introduction of artefacts were observed. The artefacts were manifested by an increase in details close to resolution limit (detectable with wavelet energy and Haralick parameters). This effect became more prominent as the compression ratio increased. By contrast, the increase of artefact formation with the ratio was smaller when wavelet denoising was used. This notion is confirmed by the fact that removal of Poisson noise from synthetic MTF data and images of periodic grating arrays prior to irreversible compression resulted only in attenuation of the highest spatial frequencies but prevented their enhancement. Therefore, the proposed denoising technique may be applied not only to increase the compression ratio of reversible coding methods but also to pre-process images before compression by irreversible algorithms. To our knowledge no similar analysis of influence of irreversible compression of microscope data has been presented by other workers.

It may be noted that images used in this work contained cell nuclei characterized by relatively simple morphology (in comparison to cytoskeleton or endoplasmic reticulum). In other words, the micrographs contained small number of objects (features) close to resolution limit (according to Rayleigh criterion). Therefore, one may postulate that compression-induced loss of biological information present in the micrographs could be greater if images comprised more objects close to resolution limit (complex morphology). One should note that the proposed denoising algorithm itself did not generate artefacts of this size and prevented their formation when irreversible coding was used. Instead, the denoising resulted in attenuation of the highest spatial frequencies (acted as a low-pass filter). However, two point sources positioned at the distance equal to the lowest of the attenuated spatial frequencies could not be resolved according to Rayleigh criterion. Furthermore, it is likely that such spatial frequencies

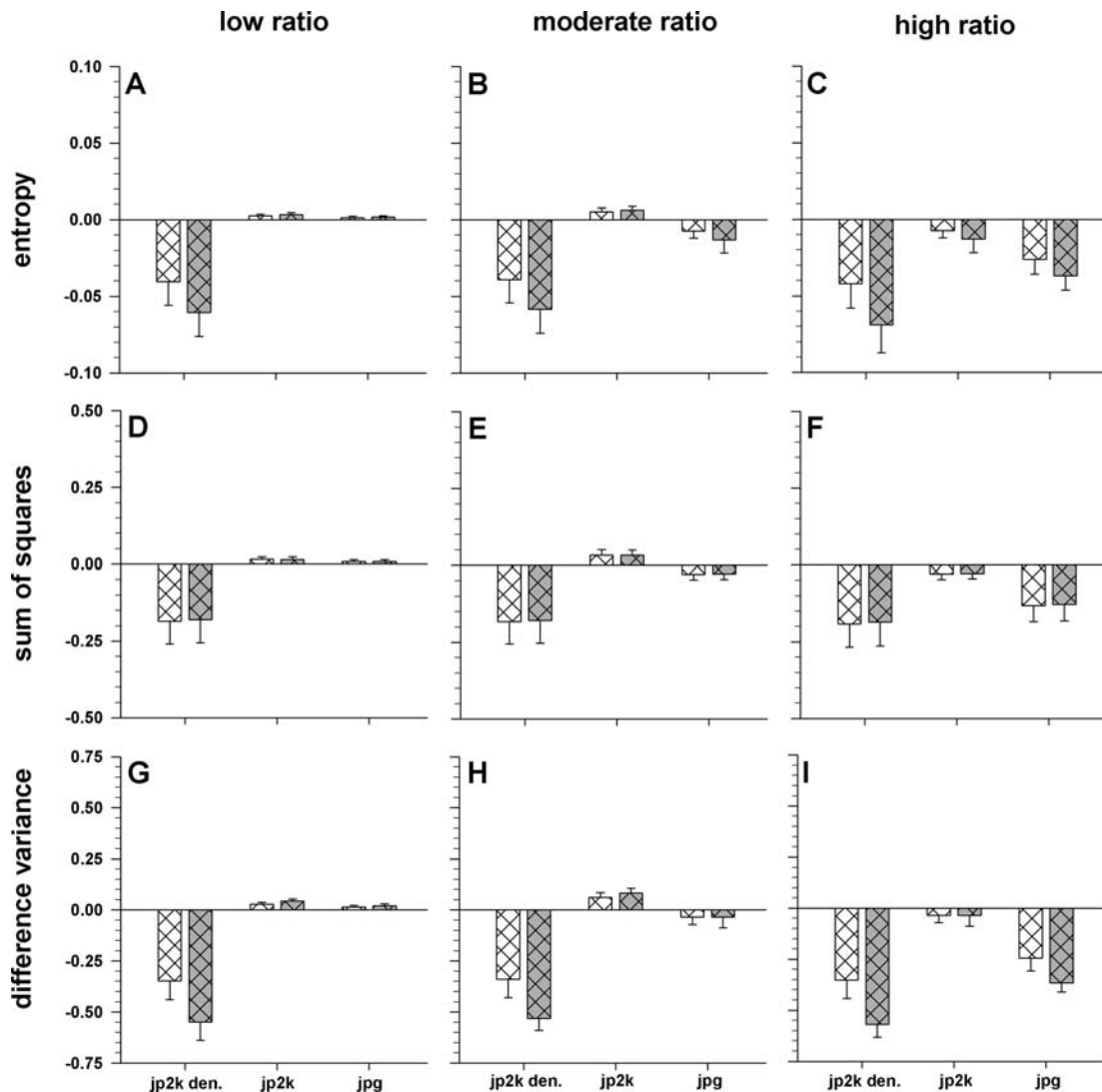


Fig. 8. Alteration of textures of PI-stained nuclei in images compressed with JPEG2000 (with and without denoising) and JPEG. The algorithms were set to provide the following absolute compression ratios: low ($2.5\times$, ADG), moderate ($7.5\times$, BEH) or high ($22.5\times$, CFI). The nuclei were analyzed using relative (see Materials and Methods) texture (Haralick) parameters: sum of squares (ABC), entropy (DEF) and difference variance (GHI). The parameters were calculated at a distance of 2 (white bars) and 5 (grey bars) pixels. The standard deviation is represented with error bars.

might not be retrieved from a biological micrograph (which does not usually contain sinusoidal patterns) owing to the presence of noise. Therefore, it is probable that the proposed denoising routine should perform at least equally well in case of biological micrographs containing objects of more complex morphology than cell nuclei. This notion is supported by our latest results, which are being prepared for a separate publication.

The approach proposed in this manuscript focusses on characteristics of input images, instead of analyzing the output of image interpretation/analysis procedures. To validate irreversible compression algorithm for microscopy applications, one may demonstrate that irreversible compression did not affect results of specified measurements

that used the images as input data (Cosman *et al.*, 1994; Tengowski, 2004). However, modern imaging techniques frequently involve automated schemes of image analysis. Therefore, logically such validation procedures should be repeated whenever biological sample, imaging system, image-registration conditions or image-analysis procedure is changed. Consequently, even though compliance of JPEG and irreversible JPEG2000 with 21 CFR part 11 can be ascertained using this approach (Cosman *et al.*, 1994; Tengowski, 2004), it may not easily be extended or generalized, and may be limited to standard, repeatable assays.

The denoising scheme proposed in this paper is similar to algorithms published previously, which comprise noise estimator and wavelet shrinkage (thresholding) scheme where

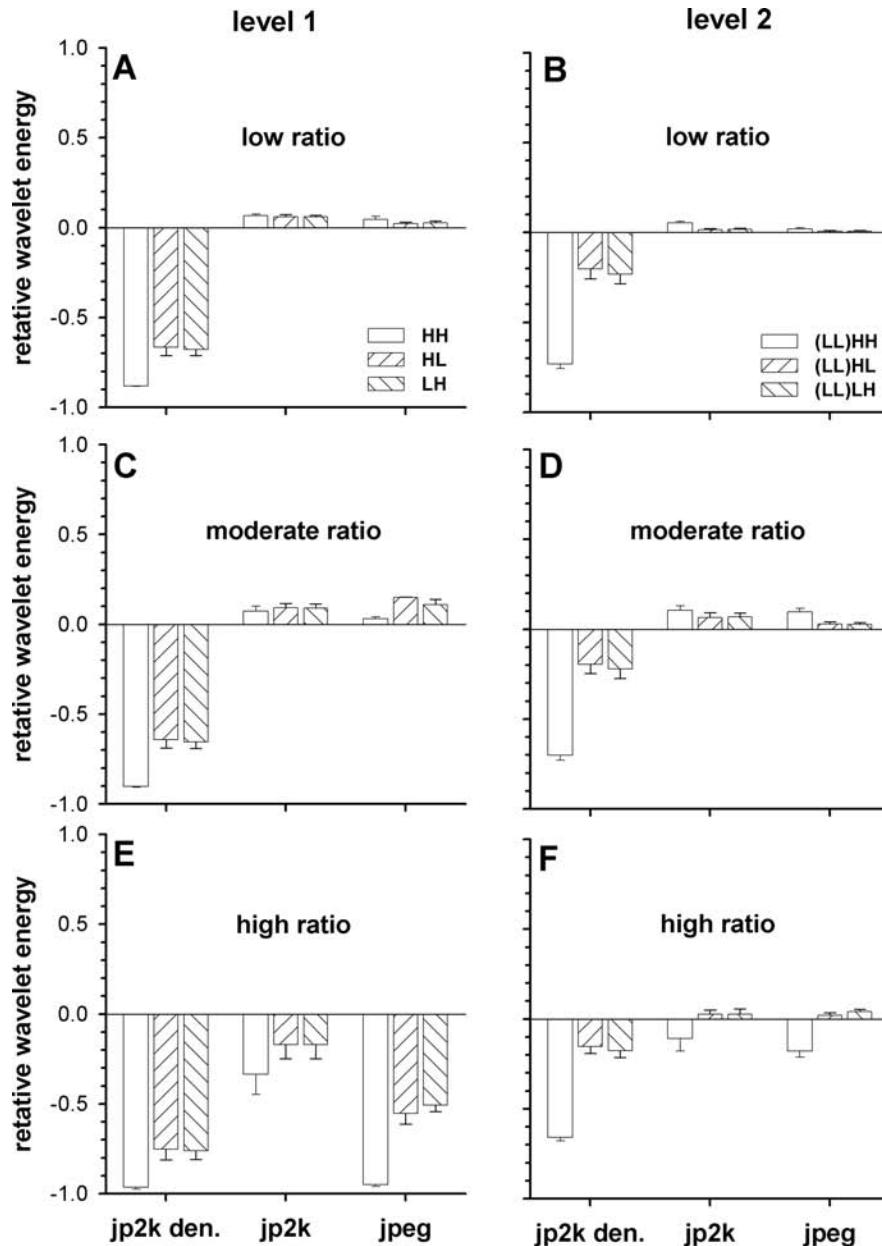


Fig. 9. Influence of irreversible compression on textures in images of PI-stained nuclei, determined using wavelet (Haar) decomposition. The images were compressed using denoising followed by JPEG2000, irreversible JPEG2000 (without denoising) and JPEG with low ($2.5\times$, AB), moderate ($7.5\times$, CD) and high ($22.5\times$, EF) absolute compression ratios. The relative wavelet energy was measured at first (ACD) and second (BEF) decomposition levels, following application of high-pass (H) and low-pass (L) filters in sequence. The standard deviation is represented with error bars.

amount of shrinkage depends on SNR (Kolaczyk, 1997; Kolaczyk, 1999b; Nowak & Baraniuk, 1999). The proposed algorithm includes an unbiased Poisson noise estimator (described in (Nowak & Baraniuk, 1999) but instead of single-step wavelet thresholding method presented in this paper an iterative bivariate wavelet technique (Sendur & Selesnick, 2002) was applied to perform image denoising. Consequently, one may not claim that the proposed denoising method is optimal in limiting case (i.e. when the number of wavelet coefficients is infinite) (Nowak, 1997; Nowak & Baraniuk,

1999). However, in a non-limiting case (finite number of coefficients corresponding to a micrograph) performance of the proposed method was similar or better compared with the former algorithm (Nowak & Baraniuk, 1999) (data not shown). Furthermore, one may expect that performance this Poisson noise estimator (Nowak & Baraniuk, 1999) combined with wavelet shrinkage should be superior to alternative methods of removal of this form of noise (Besbeas *et al.*, 2004) when signal components are broad and their edges are smooth. One should note that a band-limited microscope

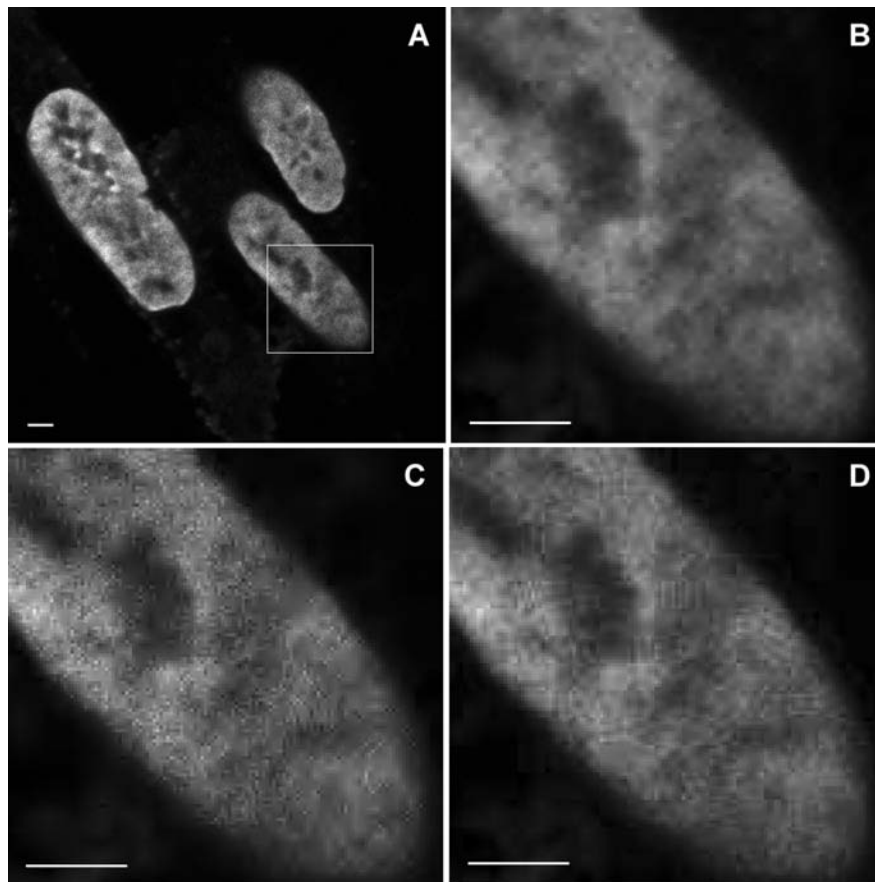


Fig. 10. Distortion in images of cell nuclei stained with PI in the course of irreversible compression. The fragment indicated with a white square (A, raw image) was magnified to show effects of compression (ratio 22.5 \times) with irreversible JPEG2000 with denoising (B) and without denoising (C) and JPEG (D). Bar – 2.5 μm .

image is sampled at Nyquist frequency is likely to represent this type of data. Another important advantage of this approach to image denoising is its flexibility. In our imaging system, photonic noise was predominant and therefore might be characterized using simple Poisson model. However, the proposed approach presented here may easily be extended to incorporate other noise sources modelled as composite (additive, power or multiplicative) functions of the signal. Examples of such extension include removal of Rician noise from NMR images (Nowak, 1999). This type of noise is signal-dependent and tends to approach Rayleigh distribution at low SNR, whereas at high SNR, its distribution is approximately Gaussian (Nowak, 1999). Composite type of noise is present also in fluorescence micrographs registered with a CCD camera (Bernas *et al.*, 2007). At low signal level, the noise is signal-independent with Gaussian distribution, whereas at high level, the noise is signal-independent and follows Poisson statistics (Bernas *et al.*, 2007). Hence, if a function of dependence between noise and signal is for a given detector, one may embed it into denoising procedure which, consequently, may be constructed so as preserve signal registered using the imaging system (microscope) equipped with this detector.

Our data do not permit us to make general statements regarding the computational complexity of the proposed method. However, the denoising procedure implemented on an entry-level desktop PC typically required 15s–18s. Therefore, we think that although the complexity is on the high side, it is not prohibitive.

The denoised images were coded using a simple scalar quantization implemented in JPEG2000 (ISO/IEC, 2002). However, our preliminary results indicate that use of more sophisticated coding techniques like SFQ (Xiong *et al.*, 1997) results in a further decrease in size of the denoised image files without information loss. Thus, one may optimize a coding/quantization procedure to take best advantage of a particular image denoising procedure.

Acknowledgement

This work was partially supported by the Foundation for Polish Science (TB) and Purdue University Cytometry Laboratories. We would like to thank Gretchen Lawler for assistance in editing the manuscript.

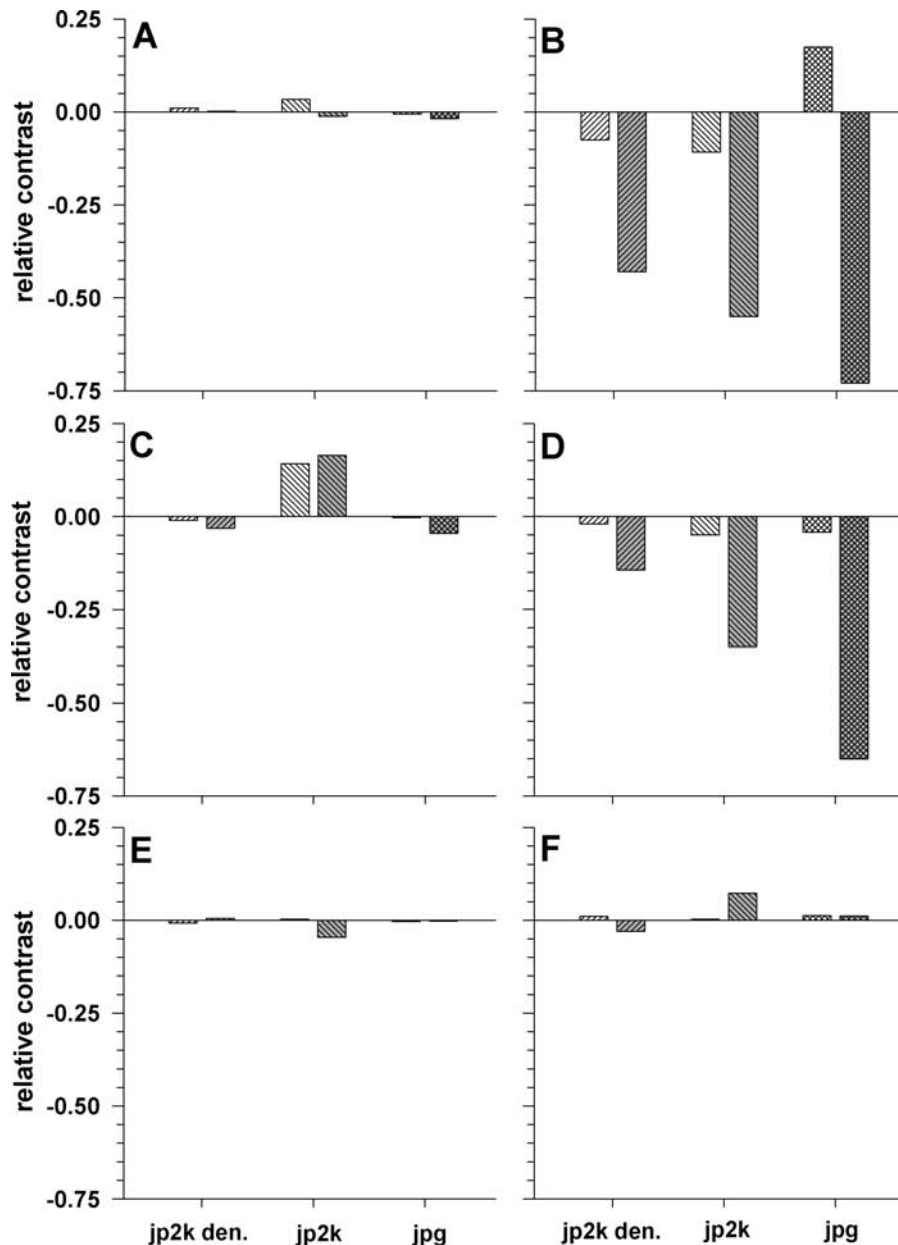


Fig. 11. Influence of irreversible compression on images of the array test pattern registered with large (average of 72.8 per pixel, white bars) and small (an average of 4.1 per pixel, dark bars) number of photons. The images were compressed with moderate ($7.5\times$, ACE) and high ($22.5\times$, BDF) absolute ratios. The fidelity of reproduction of the test pattern was estimated using relative contrast between the bright and the dark bars (see Materials and Methods). The contrast was calculated shifting the pattern with respect to itself by one bar width. The respective widths were $0.100\ \mu\text{m}$ (AB), $0.125\ \mu\text{m}$ (CD) and $0.250\ \mu\text{m}$ (EF). The wavelet denoising followed by irreversible JPEG2000 (moderate and high ratio) is shown with slash pattern. Effects of compression (with the same ratio as obtained using the denoising) using JPEG (backslash pattern) and irreversible JPEG2000 without denoising (grid pattern) are shown for comparison.

References

- Amer, A., Dubois, E. & Mitiche, A. (2002) Reliable and fast structure-oriented video noise estimation. *Proc. IEEE Int. Conf. Image Process.* **1**, 840–843.
- Bernas, T., Barnes, D., Asem, E.K., Robinson, J.P. & Rajwa, B. (2007) Precision of light intensity measurement in biological optical microscopy. *J. Microsc.* **226**, 163–174.
- Bernas, T., Rajwa, B., Asem, E.K. & Robinson, J.P. (2005a) The loss of image quality in photobleaching during microscopic imaging of fluorescent probes bound to chromatin. *J. Biomed. Opt.* **10**, 64015–64020.
- Bernas, T., Rajwa, B., Asem, E.K. & Robinson, J.P. (2006) Compression of fluorescence microscopy images based on the signal-to-noise estimation. *Microsc. Res. Tech.* **69**, 1–9.

- Bernas, T., Robinson, J.P., Darzynkiewicz, Z., Hyun, W., Orfao, A. & Rabinovitch, P. (2005b) Basics of digital microscopy. *Current Protocols in Cytometry* (ed. by J.P. Robinson), pp. 1–14. Wiley-Liss, New York.
- Bernas, T., Zarebski, M., Cook, P.R. & Dobrucki, J.W. (2004) Minimizing photobleaching during confocal microscopy of fluorescent probes bound to chromatin: role of anoxia and photon flux. *J. Microsc.* **215**, 281–296.
- Besbeas, P., Feis, I. & Sapatinas, T. (2004) A comparative simulation study of wavelet shrinkage estimators for poisson counts. *Int. Stat. Rev.* **72**, 209–237.
- CFR (2004) 21 Code of Federal Regulations part 11.
- Chang, G., Yu, B. & Vatterli, M. (2000) Adaptive wavelet thresholding for image denoising and compression. *IEEE Trans. Image Process.* **9**, 1532–1546.
- Chen, C.C. (1998) On the Selection of Image Compression Algorithms.
- Cosman, C., Gray, R.M. & Olshen, R.A. (1994) Evaluating quality of compressed medical images: SNR, subjective rating, and diagnostic accuracy. *Proc. IEEE*, **82**, 919–932.
- Donoho, D.L. (1993) Non-linear wavelet methods for recovery of signals, densities and spectra from indirect and noisy data. *Symposium in Applied Mathematics: Different Perspectives on Wavelets* (ed. by I. Daubechies). American Mathematical Society, San Antonio.
- Donoho, D.L. (1995) De-noising by soft thresholding. *IEEE Trans. Inf. Theor.* **41**, 613–627.
- Donoho, D.M. & Johnstone, J.L. (1994) Ideal denoising in an orthonormal basis chosen from a library of bases. *Comput. Rend. Acad. Sci. Paris Ser.* **319**, 1317–1322.
- Ebrahimi, F., Chamik, M. & Winkler, S. (2004) JPEG vs. JPEG2000: an objective comparison of image encoding quality. *Proc. SPIE Appl. Digital Image Process.* **5558**, 300–3008.
- Fryzlewicz, P. & Nason, G.P. (2001) Poisson intensity estimation using wavelets and the FisZ transformation. Department of Mathematics, University of Bristol, Bristol, United Kingdom.
- Grgic, S., Mrak, M., Grgic, M. & Zovko-Cihlar, B. (2003) Comparative study of JPEG and JPEG2000 image coders. *Proceedings of the 17th Conference on Applied Electromagnetics and Communications*, 109–112.
- ISO/IEC (1994) ISO/IEC, ITU-T, Information technology–Digital compression and coding of continuous-tone still images: Requirements and guidelines, ISO/IEC International Standard 10918-1 and ITU-T Recommendation T.81.
- ISO/IEC (2002) ISO/IEC, ITU-T, Information technology – JPEG 2000 image coding system: Extensions, ISO/IEC International Standard 15444-2 and ITU-T Recommendation T.801
- Kolaczyk, A.D. (1999a) Bayesian multiscale models for Poisson processes. *J. Am. Statist. Assoc.* **94**, 920–933.
- Kolaczyk, A.D. (1999b) Wavelet shrinkage estimation of certain Poisson intensity signals using corrected thresholds. *Statist. Sinica*, **9**, 119–135.
- Kolaczyk, E.D. (1997) Non-parametric estimation of Gamma-Ray burst intensities using Haar wavelets. *Astrophys. J.* **483**, 340–349.
- Materka, A. & Strzelecki, M. (1998) Texture analysis methods – a review. *COST B11 report* 1–33.
- National Electrical Manufacturers, A.N. (2004) Digital imaging and communications in medicine (DICOM) ROSSlyn.
- Nowak, R. & Baraniuk, R.G. (1999) Wavelet domain filter for photon imaging systems. *IEEE Trans. Image Process.* **8**, 1–24.
- Nowak, R.D. (1997) Optimal signal estimation using cross validation. *IEEE Sig. Proc. Lett.* **4**, 23–25.
- Nowak, R.D. (1999) Wavelet-based Rician noise removal for magnetic resonance imaging. *IEEE Trans. Image Process.* **8**, 1408–1419.
- Rumner, Y., Tomassi, C. & Leonidas, J.G. (2000) Earth mover's distance as a metric for image retrieval. *Int. J. Comput. Vis.* **40**, 99–121.
- Sendur, L. & Selesnick, I.W. (2002) Bivariate image shrinkage with local variance estimation. *IEEE Trans. Sig. Process.* **50**, 2744–2756.
- Simoncelli, E.P. (1999) Bayesian Inference in Wavelet Based Models. *Lecture Notes in Statistics* (ed. by P. Muller & B. Vidakovic), pp. 291–308. Springer-Verlag, New York.
- Stokseth, P. (1969) Properties of a defocused optical systems. *J. Opt. Soc. Am.* **59**, 1314–1421.
- Sung, M.M., Kim, H.J., Yoo, S.K., et al. (2002) Clinical evaluation of compression ratios using JPEG2000 on computed radiography chest images. *J. Digit. Imaging* **15**, 78–83.
- Tengowski, M.W. (2004) Image compression in morphometry studies requiring 21 CFR Part 11 compliance: procedure is key with TIFFs and various JPEG compression strengths. *Toxicol. Pathol.* **32**, 258–263.
- Timmermann, K.E. & Nowak, R.D. (1999) Multiscale modeling and estimation of Poisson processes with applications to photon-limited imaging. *IEEE Trans. Inf. Theor.* **45**.
- Tuceryan, M., Jain, A.K., Chen, C.H. & Pau, L.F.W.P.S.P. (1998) Texture analysis. *Handbook of Pattern Recognition and Computer Vision*, 2nd edn (ed. by C.H. Chen & P.S.P. Wang), pp. 207–248. World Scientific Publishing Co, New York.
- Wohlberg, B. & de Jager, G. (1999) A review of the fractal image coding literature. *IEEE Trans. Image Process.* **8**, 1716–1729.
- Wong, S., Zaremba, L., Gooden, D. & Huang, H.K. (1995) Radiologic image compression-a review. *Proc. IEEE* **83**, 194–219.
- Xiong, Z., Ramchandran, K. & Orchard, M.T. (1997) Space-frequency quantization for wavelet image coding. *IEEE Trans. Image Proc.* **6**, 677–693.